

Integrating Seismic and Infrasound Technologies for Discriminating Tectonic and Quarry Explosions in Southeastern Brazil

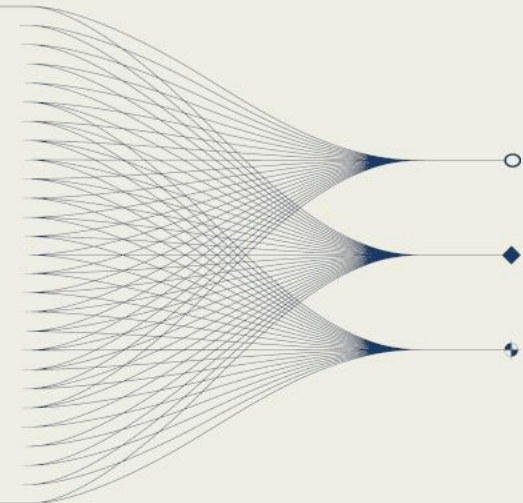
D. Fontenele, L. Barros, G. Marotta, and L. Assunção

University of Brasília – Brazil



INTRODUCTION AND MAIN RESULTS

The Sete Lagoas region (Brazil) experiences both low-magnitude earthquakes and quarry blasts within a complex karst and mining setting, making classification challenging. This study investigates the joint use of seismic and infrasound observations to better discriminate natural from anthropogenic events and advance knowledge of local seismicity. The approach demonstrated effective results, as blasts invariably radiate acoustic signals, thereby improving event discrimination, strengthening hazard assessment, and paving the way for automated classification.



INTRODUCTION

The Sete Lagoas region (Minas Gerais, Brazil) hosts both low-magnitude tectonic events (SISBRA, USP-IG and UnB, 2022) and quarry blasts within a complex karstic setting and intense mining activity (Galvão et al., 2016; Galvão et al., 2024) (Fig. 1). Although seismicity has been reported since at least 1939, its causes remain insufficiently constrained. Events are typically isolated—showing no foreshocks or aftershocks and long interevent intervals—which suggests non-classical tectonic mechanisms. The coexistence of natural and anthropogenic sources, along with limited operational data from mining companies, complicates reliable classification.

Several seismic discriminants have been proposed, including spectral analysis (Postema, 1996; Korrat et al., 2022), P/S amplitude ratios (Wang et al., 2020), source parameters (Saadalla et al., 2023), and magnitude comparisons (Holt, 2021), with mixed reliability. Infrasound provides a complementary constraint because quarry blasts commonly radiate detectable atmospheric signals, unlike many low-magnitude earthquakes (Ghica et al., 2016; Mutschlecner & Whitaker, 2005; Arrowsmith et al., 2011). This technology has been widely adopted by the Comprehensive Nuclear-Test-Ban Treaty Organization

(CTBTO) through its International Monitoring System (IMS) (Hupe et al., 2022), but remains underutilized in Brazil, with limited instrumentation (Fontenele, 2023) and scarce scientific output (Joshi et al., 2018). This study explores the integration of seismic and infrasound observations to discriminate sources in Sete Lagoas, with the goal of improving event classification and advancing understanding of local seismicity.

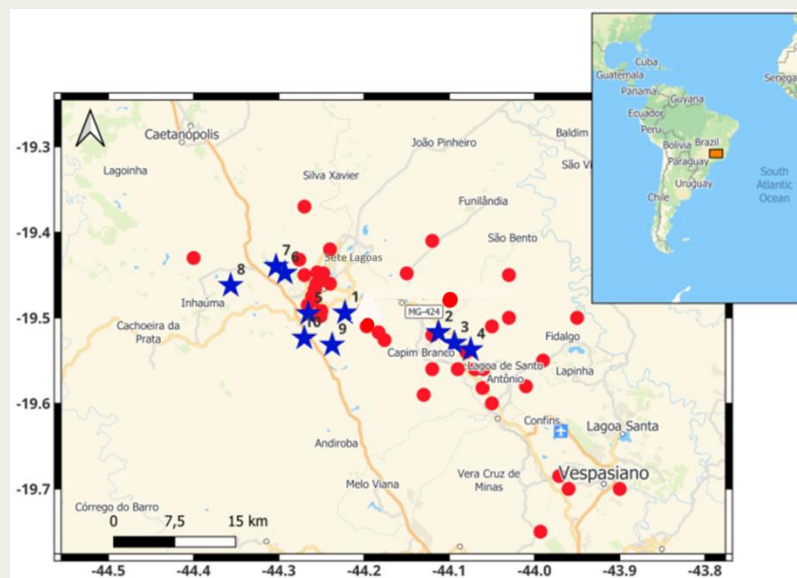


Fig. 1 - Circles indicate the epicenters of natural events that occurred between 1939 and 2022 (IAG-USP and SIS-UnB catalogs). Stars denote the locations of active mines.

METHOD

Event location accuracy is determined by several factors, including the number and spatial distribution of stations, signal-to-noise ratio (SNR), timing precision, and the representativeness of the velocity model used for the region. Among these, the number and geometry of stations are the most critical, as they directly control azimuthal coverage and overall network resolution. Our initial deployment strategy was designed to surround the epicentral area and distribute instruments across multiple quadrants, thereby reducing the azimuthal gap and improving network geometry (Lay & Wallace, 1995; Havskov & Alguacil, 2016). Within the limits imposed by logistics, we installed eleven stations: broadband triaxial seismic stations and hybrid stations integrating a vertical short-period seismometer with a microbarometer (HDF channels, used here as infrasound/acoustic channels). In addition, we deployed a four-element infrasound array of hybrid stations, with inter-sensor spacing of ~100–200 m, to enhance the detection and characterization of atmospheric signals from local surface sources (Fig. 2).

RESULTS

To mitigate wind-induced turbulence noise, each microbarometer was coupled with a passive wind-noise reduction filter consisting of a polyurethane foam block ($\approx 10 \times 10 \times 10$ cm) covered with No. 1 gravel (~ 19 mm). A plastic tube (inner diameter ≈ 6.35 mm, length ≈ 1 m) was inserted through the filter and connected to the microbarometer inlet (Fig. 3).

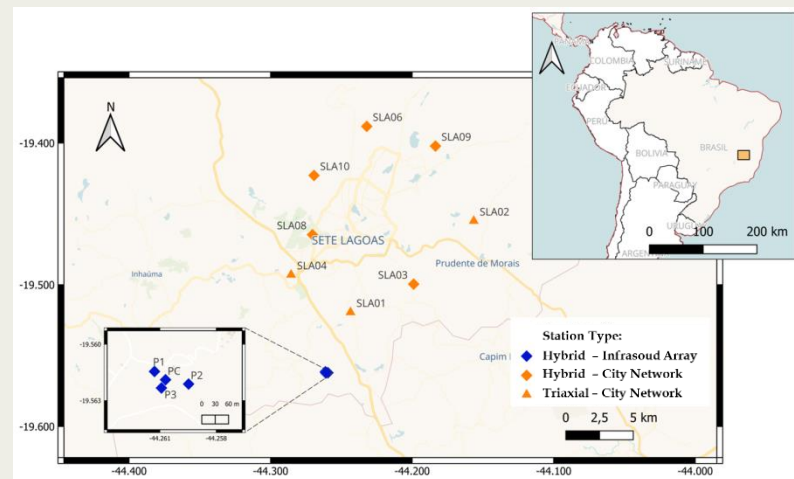


Fig. 2 – Location of triaxial seismic stations (orange triangles) and hybrid stations (orange and blue diamonds), as well as their distribution, forming the City Network (orange symbols) and the Infrasound Array (blue symbols) in the Sete Lagoas/MG region.

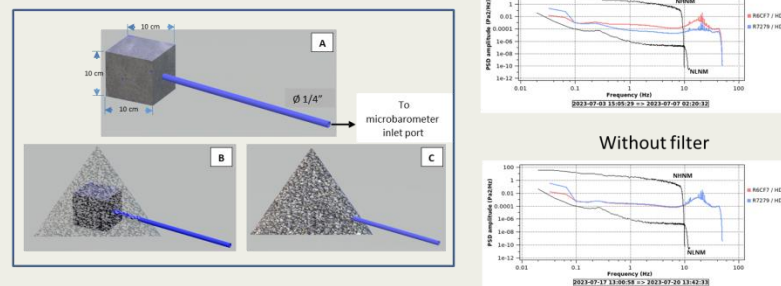


Fig. 3 - Filter developed to reduce wind noise: **A)** Polyurethane foam with an inserted plastic tube; **B,** **C)** Layer of gravel covering the foam. The plastic tube connects to the barograph sensor's inlet port (not shown in the figure).

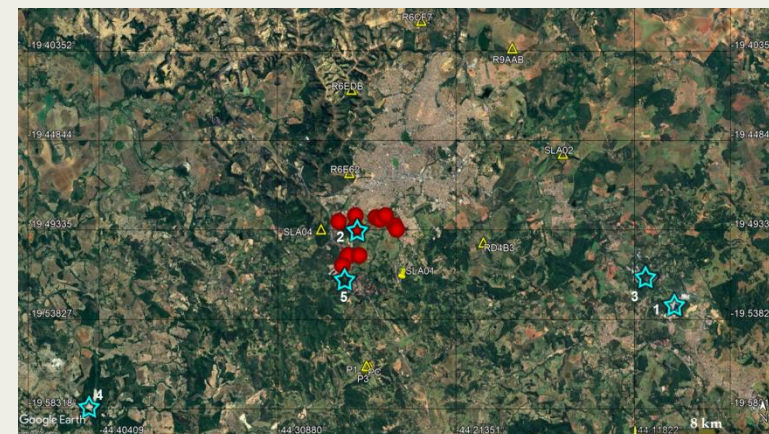


Fig. 4 – Circles mark the epicenters of natural events recorded in 2024 by seismic stations in Sete Lagoas (triangles). Stars indicate the locations of quarry blasts, which correspond to the five explosion examples analyzed in this study. P1–P4 represent the infrasound array (P1 = R7279, P2 = R6E11, P3 = R6DF9, and PC = R4061).



Explosion-class events (Figs. 5–9)

Events were classified as blasts based on three criteria: (i) positive polarity of the first P-wave arrival, (ii) occurrence on days/times typical of quarry operations, and (iii) epicentral locations within or adjacent to mining pits. In the HDF channels (microbarometer) records at each station, we observed acoustic signals arrivals whose onset times are consistent with the expected delay relative to the first P-wave arrival recorded on the EHZ component, given the sound propagation velocity and the source-to-station distance.

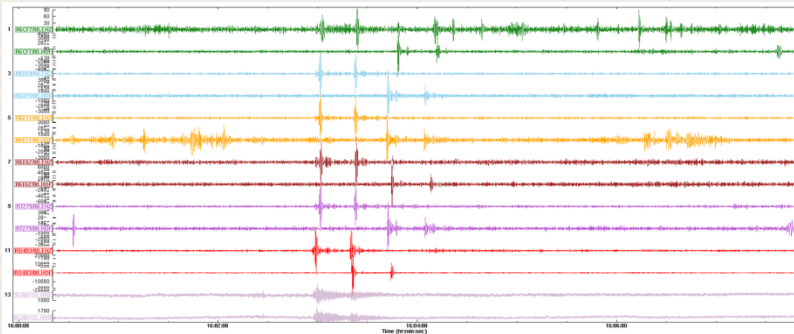


Fig. 5 – Event on 22 April 2024 at 16:02:54 UTC, M 1.4 (Mine #1).

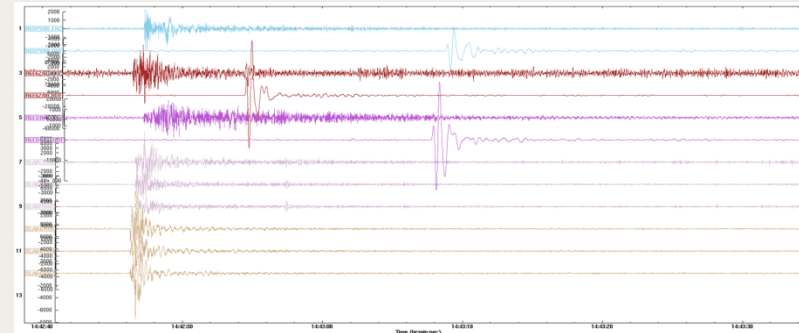


Fig. 6 – Event on 28 May 2024 at 14:42:46 UTC, M 1.6 (Mine #2).

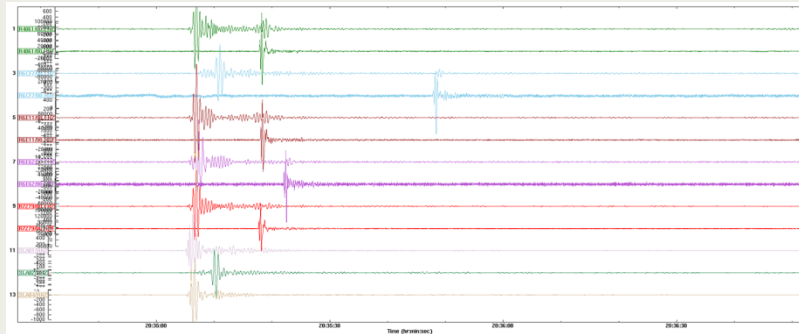


Fig. 7 – Event on 11 June 2024 at 20:35:02 UTC, M 2.0 (Mine #3).

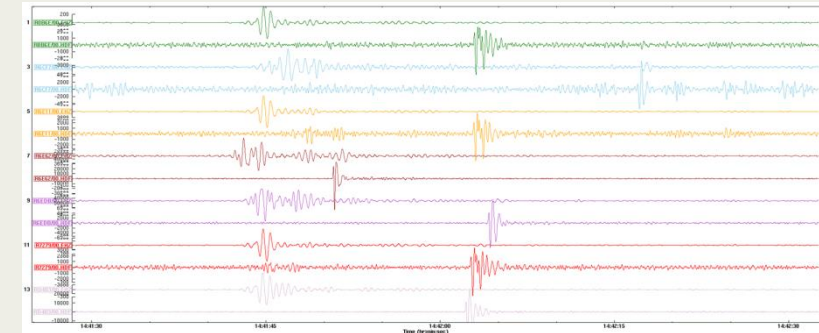


Fig. 8 – Event on 24 October 2024 at 14:41:40 UTC, M 1.5 (Mine #4).

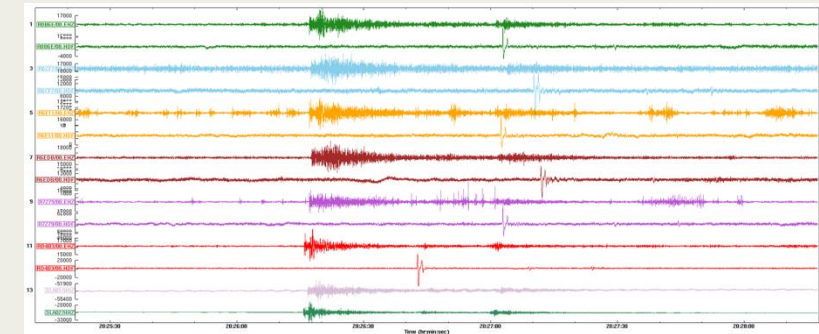


Fig. 9 – Event on 18 November 2024 at 20:26:13 UTC, M 1.6 (Mine #5).



Tables (Figs. 5–9).

The tables below summarize the blast events. Because these are open-pit quarry explosions, **depths were set to zero**.

Event dd/mm/yyyy	Station Code	P-wave hh:mm:ss.ss	Acoustic-wave - P-wave Time Difference (sec)	Acoustic Wave Velocity (km/s)	Epicentral Distance (km)
22/04/2024 16:02:53.52 UTC M 1.4	R6CF7	16:02:57.90	49.1	0.43	23.0
	R6DF9	16:02:57.60	42.6	0.42	19.5
	R6E11	16:02:57.60	42.6	0.42	19.5
	R6E62	16:02:57.70	45.9	0.44	22.0
	RD4B3	16:02:56.40	24.3	0.51	13.8
	R7279	16:02:57.60	42.6	0.42	19.5

28/05/2024 14:42:46.21 UTC M 1.6	R6DF9	14:42:47.20	21.5	0.32	7.3
	R6EDB	14:42:47.20	20.5	0.34	7.3
	R6E62	14:42:46.40	8.1	0.37	3.1

11/06/2024 20:35:02.29 UTC M 2.3	R6CF7	20:35:06.70	43.0	0.60	28.3
	R4061	20:35:05.20	12.5	1.02	15.7
	R6E11	20:35:05.20	12.5	1.02	15.7
	R6E62	20:35:05.60	16.4	0.98	19.4
	R7279	20:35:05.20	12.5	1.02	15.7

24/10/2024 14:41:40.80 UTC M 1.6	R6CF7	14:41:43.40	32.9	0.35	12.6
	R6EDB	14:41:42.30	21.5	0.36	8.2
	R6E62	14:41:41.80	8.9	0.36	3.6
	R7279	14:41:42.20	20.0	0.33	7.0
	ROB6E	14:41:42.20	20.0	0.33	7.0
	R6E11	14:41:42.20	20.0	0.33	7.0

18/11/2024 20:26:14.18 UTC M 1.5	R6CF7	20:26:17.40	53.3	0.33	18.5
	R6E11	20:26:17.00	45.2	0.33	15.9
	R6E62	20:26:17.20	48.5	0.33	17.0
	R6EDB	20:26:17.40	54.0	0.33	19.0
	RD4B3	20:26:15.90	26.4	0.32	8.9
	R7279	20:26:17.00	45.2	0.33	15.9

Tectonic-class events (Figs. 10–14)

Events were classified as tectonic based on: (i) variations in the polarity of the first P-wave arrival, (ii) hypocentral depth, and (iii) epicentral location. In all HDF records, **no signals of acoustic origin** were observed. The time windows displayed for each event are sufficient to reveal such arrivals—had they been present—given the speed of sound and the epicenter–station distances.

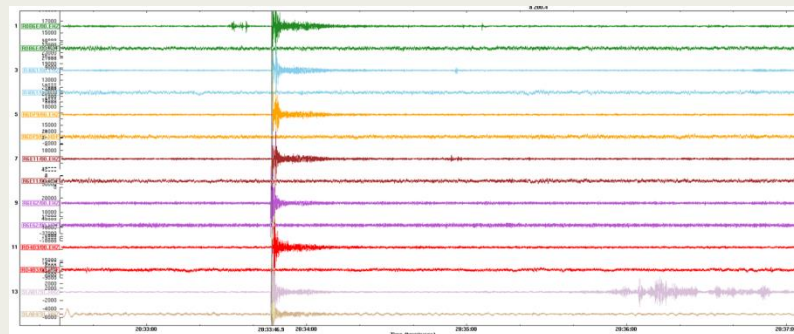


Fig. 10 – Event on 1 March 2024 at 20:33:45 UTC, M 1.4.

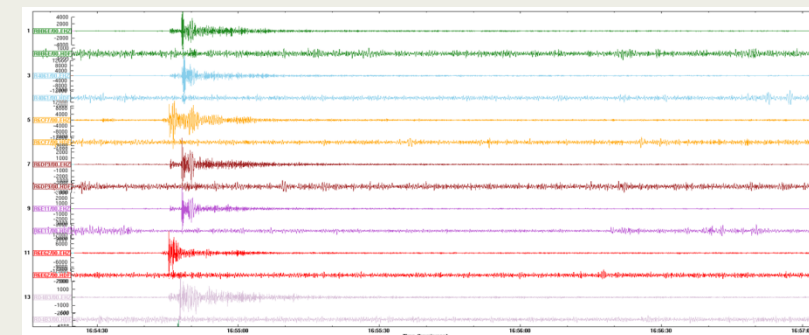


Fig. 11 – Event on 2 March 2024 at 16:54:41 UTC, M 2.5.

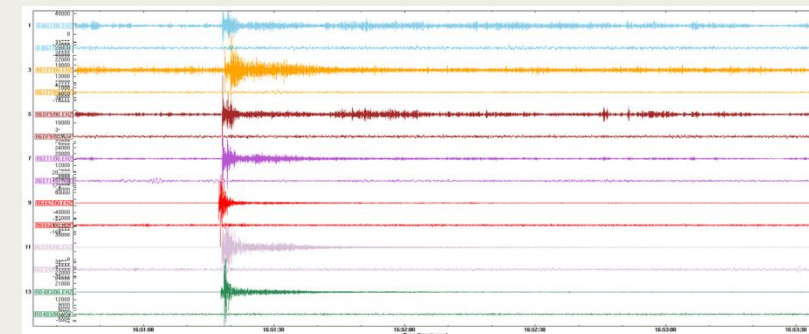


Fig. 12 – Event on 4 March 2024 at 16:51:16 UTC, M 2.1.



CONCLUSION

The absence of acoustic (infrasound) signal records in events may serve as a simple yet robust discriminant, since quarry blasts invariably generate such signals. This study demonstrated that this criterion is effective as a supporting tool in the challenging task of distinguishing tectonic events from anthropogenic sources, particularly quarry blasts associated with open-pit mining. Beyond its scientific significance, the approach has practical implications for seismic monitoring and hazard assessment in Brazil, especially in regions affected by mining activity. Future work will focus on developing and validating an algorithm to automate event classification in the Sete Lagoas region, evaluating its performance against events characterized through the joint analysis of seismic and infrasound data, thereby strengthening the integration of these observations and offering potential applications to similar contexts in other regions.

Tables (Figs. 10–14).

The tables below summarize these tectonic events. Since no acoustic signals were recorded, we do not report infrasound velocity or Acoustic–P-wave Time Difference (s) for these cases.

Event dd/mm/yyyy	Station Code	P-wave hh:mm:ss.ss	Expected Acoustic-Wave Arrival Time	Epicentral Distance (km)
01/03/2024 20:33:45.39 UTC M 1.4 2.8 km depth	R0B6E	20:33:47.20	20:34:08.04	7.7
	R6DF9	20:33:47.20	20:34:08.04	7.7
	R6E11	20:33:47.20	20:34:08.04	7.7
	R6E62	20:33:46.50	20:33:56.86	3.9
	R4061	20:33:47.20	20:34:08.04	7.7
	RD4B3	20:33:46.90	20:34:00.10	5.0
02/03/2024 16:54:41.47 UTC M 2.5 8.6 km depth	R6CF7	16:54:43.90	16:54:57.68	5.5
	R6DF9	16:54:45.40	16:55:23.61	14.3
	R6E11	16:54:45.40	16:55:23.61	14.3
	R6E62	16:54:43.80	16:54:54.44	4.4
	R0B6E	16:54:45.40	16:55:23.61	14.3
	RD4B3	16:54:45.10	16:55:13.89	11.0
	R4061	16:54:45.40	16:55:23.61	14.3
04/03/2024 16:51:16.24 UTC M 2.1 2.6 km depth	R6CF7	16:51:18.60	16:51:50.06	11.5
	R6DF9	16:51:18.10	16:51:38.89	7.7
	R6E11	16:51:18.10	16:51:38.89	7.7
	R6E62	16:51:17.30	16:51:25.65	3.2
	R6EDB	16:51:18.00	16:51:38.89	7.7
	RD4B3	16:51:17.70	16:51:33.59	5.9
	R4061	16:51:18.10	16:51:38.89	7.7
19/05/2024 19:15:16.28 UTC M 1.8 3 km depth	R6CF7	19:15:18.80	19:15:50.69	11.7
	R7279	19:15:18.10	19:15:37.46	7.2
	R6E11	19:15:18.10	19:15:37.46	7.2
	R6E62	19:15:17.40	19:15:28.93	4.3
	R4061	19:15:18.10	19:15:37.46	7.2
07/06/2024 07:06:12.63 UTC M 1.0 2.7 km depth	R6CF7	07:06:15.00	07:06:47.34	11.8
	R6E11	07:06:14.40	07:06:33.81	7.2
	R6E62	07:06:13.70	07:06:22.63	3.4
	R7279	07:06:14.40	07:06:33.81	7.2

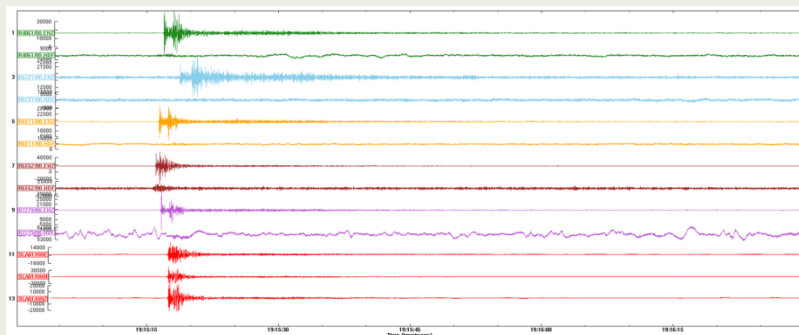


Fig. 13 – Event on 19 May 2024 at 19:15:16 UTC, M 1.7.

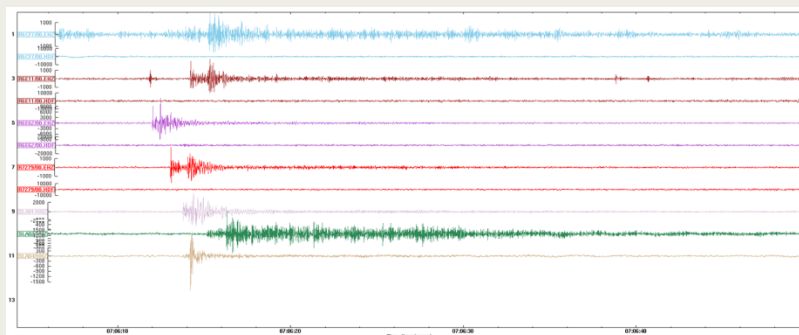


Fig. 14 – Event on 7 June 2024 at 07:06:10 UTC, M 1.0.

REFERENCES

Arrowsmith, S. J., Whitaker, R. W., & Stead, R. J. (2011). Infrasound as a depth discriminant. *Los Alamos National Laboratory Report*, LA-UR-11-00689.

Fontenele, D. P. (2023). *Melhoria na capacidade de detecção da estação infrassônica de Brasília e discriminação de eventos tectônicos de explosões em pedreiras, utilizando a tecnologia infrassônica* [Master's thesis, Universidade de Brasília – UnB]. Instituto de Geociências – IG.

Galvão, P., Hirata, RT., Cordeiro, A., Barbat, D., & Peñaranda, J. (2016). *Geologic conceptual model of the municipality of Sete Lagoas (MG, Brazil) and the surroundings*. *An Acad Bras Cienc.* 2016 Mar;88(1):35-53. doi: 10.1590/0001-3765201520140400. Epub 2016 Feb 2.

Galvão, P.; Schuch, C.; Pereira, S.; de Oliveira, J.M.; Assunção, P.; Conicelli, B.; Halihan, T.; de Paula, R. (2024). *Modeling the Impact of Groundwater Pumping on Karst Geotechnical Risks in Sete Lagoas (MG), Brazil*. *Water* 2024, 16, 1975. <https://doi.org/10.3390/w16141975>.

Ghica, D. V., Popa, M., Grecu, B., & Radulian, M. (2016). Identification of blasting sources in the Dobrogea seismogenic region, Romania, using seismo-acoustic signals. *Physics and Chemistry of the Earth*, 95, 125–134.

Havskov, J., & Alguacil, G. (2016). Seismic arrays. In *Instrumentation in earthquake seismology* (pp. 309–329).

Holt, M. M. (2021). *Seismic discrimination of earthquakes and explosions using comparisons of local magnitude (ML) and coda magnitude (MC)* (Doctoral dissertation, The University of Utah).

Hupe, P., Ceranna, L., Le Pichon, A., Matoza, R. S., & Mialle, P. (2022). International monitoring system infrasound data products for atmospheric studies and civilian applications. *Earth System Science Data Discussions*, 2022, 1-40.

Joshi, L. M., Sripathi, S., Kumar, M. R., & Kherani, E. A. (2018). Simulating the dependence of seismo-ionospheric coupling on the magnetic field inclination. *Annales Geophysicae*, 36(1), 25–35. <https://doi.org/10.5194/angeo-36-25-2018>

Korrat, I. M., Lethy, A., Elgabry, M. N., Hussein, H. M., & Othman, A. S. (2022). Discrimination between small earthquakes and quarry blasts in Egypt using spectral source characteristics. *Pure and Applied Geophysics*, 179, 599–618. <https://doi.org/10.1007/s00024-022-02953-w>

Lay, T., & Wallace, T. C. (1995). *Modern global seismology* (Vol. 58). Academic Press.

Mutschlecner, J. P., & Whitaker, R. W. (2005). Infrasound from earthquakes. *Journal of Geophysical Research: Atmospheres*, 110(D1). <https://doi.org/10.1029/2004JD005067>

Postema, M. A. B. (1996). *Discrimination between quarry blasts and micro-earthquakes using spectral analysis, applied to local Israeli events* [Master's thesis, University of Utrecht]. 41 pp.

Saadalla, H., Abdelhafez, H. E., & Hayashida, T. (2023). Discrimination between earthquakes and quarry blasts in the Aswan region, southern Egypt, using P-wave source spectra. *Journal of Seismology*, 27, 279–289. <https://doi.org/10.1007/s10950-023-10143-x>

Wang, R., Schmandt, B., & Kiser, E. (2020). Seismic discrimination of controlled explosions and earthquakes near Mount St. Helens using P/S ratios. *Journal of Geophysical Research: Solid Earth*, 125(11), e2020JB020338. <https://doi.org/10.1029/2020JB020338>